Geometrical exponents of contour loops on synthetic multifractal rough surfaces: Multiplicative hierarchical cascade p model

S. Hosseinabadi,[1] M. A. Rajabpour,[2] M. Sadegh Movahed,[3,4,6] and S. M. Vaez Allaei[5,6]
[1]*Department of Physics, Alzahra University, P. O. Box 19938, Tehran 91167, Iran*
[2]*SISSA and INFN, Sezione di Triestevia Bonomea 265, 34136 Trieste, Italy*
[3]*Department of Physics, Shahid Beheshti University, G. C., Evin, Tehran 19839, Iran*
[4]*School of Astronomy, Institute for Studies in theoretical Physics and Mathematics, P. O. Box 19395-5531, Tehran, Iran*
[5]*Department of Physics, University of Tehran, Tehran 14395-547, Iran*
[6]*The Abdus Salam International Centre for Theoretical Physics, Strada Costiera 11, I-34013 Trieste, Italy*
(Received 27 July 2011; published 13 March 2012)

In this paper, we study many geometrical properties of contour loops to characterize the morphology of synthetic multifractal rough surfaces, which are generated by multiplicative hierarchical cascading processes. To this end, two different classes of multifractal rough surfaces are numerically simulated. As the first group, singular measure multifractal rough surfaces are generated by using the p model. The smoothened multifractal rough surface then is simulated by convolving the first group with a so-called Hurst exponent, H^*. The generalized multifractal dimension of isoheight lines (contours), $D(q)$, correlation exponent of contours, x_l, cumulative distributions of areas, ξ, and perimeters, η, are calculated for both synthetic multifractal rough surfaces. Our results show that for both mentioned classes, hyperscaling relations for contour loops are the same as that of monofractal systems. In contrast to singular measure multifractal rough surfaces, H^* plays a leading role in smoothened multifractal rough surfaces. All computed geometrical exponents for the first class depend not only on its Hurst exponent but also on the set of p values. But in spite of multifractal nature of smoothened surfaces (second class), the corresponding geometrical exponents are controlled by H^*, the same as what happens for monofractal rough surfaces.

DOI: 10.1103/PhysRevE.85.031113 PACS number(s): 05.45.Df, 47.27.eb

I. INTRODUCTION

Random phenomena in nature generate ubiquitously fractal structures that show self-similar or self-affine properties [1–4]. When the fractal structure of a system is uniform and free of irregularities, we have a monofractal structure. A monofractal system can be characterized by a single scaling law with one scaling exponent in all scales. For a self-affine surface and interface, this exponent is called *roughness exponent* or *Hurst* exponent (H). A surface with larger H seems locally smoother than the surface with smaller H [2,3].

In topics ranging from biology [5,6], surface sciences [7–10], turbulence [11–13], diffusion-limited aggregation [14], bacterial colony growth [15], climate indicators [16], to cosmology [17], there are many surfaces and interfaces that exhibit multifractal structures. A multifractal system can be considered a combination of many different monofractal subsets [2,3]. Multifractality manifests itself in systems with different scaling properties in various regions of the system. In addition, multifractals can be described by infinite different numbers of scaling exponents $h(q)$, where q can be a real number. The appearance of infinite different numbers ensures that the theoretical and numerical studies of multifractal surfaces is more complicated than those of monofractal ones. Changing one of the $h(q)$'s can lead to different feature in the system. One of the important characteristics of the multifractality is the presence of the singularity spectrum, $f(\alpha)$, which associates the Husdorff dimension $f(\alpha)$ to the subset of the support of the measure μ, where the Hölder exponent is α; in other words, $f(\alpha) = \dim_H\{x|\mu(B_x(\epsilon)) \sim \epsilon^h\}$, where $B_x(\epsilon)$ is an ϵ-box centered at x.

A single scaling exponent can be determined for a monofractal structure by use of various methods [2,6,18–22]. Not only a spectrum of exponents but also different algorithms should be computed for a multifractal feature (power spectral, distribution method, and so on) and these may give different results for a typical multifractal case [23]. Thus, the better and more complete the theoretical framework, the better our understanding, providing deeper insight into observational multifractal rough surfaces.

Recently, isoheight contour lines have been utilized to explore the topography of rough surfaces and they have exhibited interesting capabilities [24–31]. The contour plot consists of closed nonintersecting lines in the plane that connects points of equal heights. The fractal properties of the contour loops of the rough surfaces can be described by just the Hurst exponent [30,31]. This result was confirmed in different systems with quite different structures in recent years both experimentally and numerically. Using a numerical approach, the predicted relations were confirmed in glassy interfaces and turbulence [32], in two-dimensional fractional Brownian motion [26], in KPZ surfaces [25], and in discrete scale-invariant rough surfaces [27]. The predictions were also confirmed by using experimental data coming from the AFM analysis of WO(3) surfaces [24].

However, although there have been many studies concerning the contour lines of monofractal rough surfaces, there are neither theoretical nor numerical inferences about the contour lines of multifractal rough surfaces. Because of the presence of numerous exponents in the multifractal surfaces, theoretical study of multifractal surfaces seems to be difficult. Moreover, in many previous methods, the exponents determined by fractal analysis generally provide information about the average global properties, whereas geometrical analysis addresses information from point to point. J. Kondev *et al.* pointed out that geometrical characteristics can discriminate various monofractal rough surfaces that have a similar power spectrum [31,33]. Therefore, the geometrical properties may introduce a new opportunity to characterize multifractal surfaces.

It is worth noting that because contour sets are the intersection of a horizontal surface in a particular height fluctuation and do not reflect the full properties of fluctuations in various scales, it is not trivial that the geometrical properties of multifractal rough surfaces based on the isoheight nonintersecting feature behave in a multifractal manneras well. Therefore, we use a new approach to investigate these processes.

In this paper, we try to investigate multifractal structures utilizing contour loops. We study the multifractal properties of a particular kind of multifractal surfaces. Two different types of synthetic multifractal rough surfaces, namely singular measure and smoothened features, are generated. Two mentioned types have a multifractal nature. Despite the complex nature of the model, the hyperscaling relation is satisfied for both categories. In addition, from a contouring analysis, all geometrical exponents for various smoothened multifractal rough surfaces are controlled by the corresponding so-called Hurst exponent, H^*. This is also what happens for monofractal cases. However, for a singular measure multifractal rough surface, geometrical exponents depend on the set of p values that is used to generate the underlying rough surface based on the multiplicative cascade model.

The structure of the paper is as follows. In the next section we will review multifractal rough surfaces. The hierarchical model to generate the surfaces will also given in this section. The multifractal detrended fluctuation analysis in two dimensions that is used to characterize the multifractal properties of rough surfaces will be explained in Sec. III. In Sec. IV, nonlinear scaling exponents of multifractal rough surfaces are introduced. Section V will be devoted to numerical results for determining the scaling exponents of the contour loops in multifractal rough surfaces. In the last section we will summarize our findings.

II. MULTIFRACTAL ROUGH SURFACE SYNTHESIS

Recently, there has been an increasing interest in the notion of multifractality because of its extensive applications in different areas such as complex systems in industrial and natural phenomena. Dozens of methods for the synthesis of multifractal measures or multifractal rough surfaces have been invented. One of the most common methods that can be followed deterministically and stochastically is the multiplicative cascading process [4,11,22,34]. Some of these synthesis methods are known as the random β model [12], α model [35], log-stable models, log-infinitely divisible cascade models [36,37], and p model [11]. They were successfully applied in the studies related to rain in one dimension, clouds in two dimensions, and landscapes in three dimensions, as well as many other fields [36–39].

The p-model method was proposed to mimic the kinetic energy dissipation field in fully developed turbulence [11]. The so-called p model represents the spatial version of the weighted curdling feature and is known as a conservative cascade. It is based on Richardson's picture of energy transfer from cores to fine scales based on splitting eddies in a random way [40]. In this model there is no divergency in corresponding moments, in contrast to the so-called hyperbolic of the α model [11,41].

On the other hand, many scaling exponents of this model can be determined analytically; therefore, it is a proper method to simulate synthetic multifractal processes ranging from surface sciences and astronomy to high-energy physics, such as cosmology and particle physics, e.g., QCD parton shower cascades, and cosmic microwave background radiation [42–44]. In the context of the p model simulating a synthetic one-dimensional data set, consider an interval with size L. Divide L into two parts with equal lengths. The value of the left half corresponds to the fraction $0 \leqslant p \leqslant 1$ of a typical measure μ while the right-hand segment is associated to the remaining fraction $(1-p)$. By increasing the resolution to 2^{-n}, the multiplicative process divides the population in each part in the same way (see the upper panel of Fig. 1).

To simulate a mock multifractal rough surface in two dimensions, one can follow the same procedure as above. Starting from a square, one breaks it into four subsquares of the same sizes. The associated measures for each cell at this step are $p_1\mu$ for the upper right cell, $p_2\mu$ for the upper left cell, $p_3\mu$ for the lower right cell, and $p_4\mu$ for the lower left cell. The conservation of probability at each cascade step is $p_1+p_2+p_3+p_4=1$. This partitioning and redistribution process repeats and we obtain, after many generations, say n, $2^n \times 2^n$ cells of size $l/L = 2^{-n}$ (see lower panel of Fig. 1). In the stochastic approach, the fraction of measure for each subcell at an arbitrary generation is determined by a random variable $\mathcal{A}$ with a definite probability distribution function $P(\mathcal{A})$. By redistribution of measure, based on independent realization of the random $\mathcal{A}$ at smaller scales, one can generate a random singular measure over a substrate with size $L \times L$ as

$$\mu_n(\mathbf{r};l) = \mu \prod_{i=1}^{n(l)} \mathcal{A}_i(\mathbf{r}), \quad n(l) = \log_2\left(\frac{L}{l}\right) \to \infty, \tag{1}$$

where $\mathbf{r}$ shows the coordinate of the underlying cell with size l. In this work, we rely on the stochastic version of the cascade p model to generate the synthetic two-dimensional multifractal rough surface (see Figs. 2 and 3). The probability distribution function for our approach is given by

$$P(\mathcal{A}) = \tfrac{1}{4}[\delta(\mathcal{A}-\mathcal{A}_1) + \delta(\mathcal{A}-\mathcal{A}_2) + \delta(\mathcal{A}-\mathcal{A}_3) + \delta(\mathcal{A}-\mathcal{A}_4)], \tag{2}$$

where

$$\mathcal{A}_1 = p_1, \quad \mathcal{A}_2 = p_2, \quad \mathcal{A}_3 = p_3, \quad \mathcal{A}_4 = p_4. \tag{3}$$

The so-called multifractal scaling exponent, $\tau(q)$, and the generalized Hurst exponent, $h(q)$, are quantities that represent the multifractal behaviors of rough surfaces (see Sec. III for more details). For the p-model cascade, these exponents can

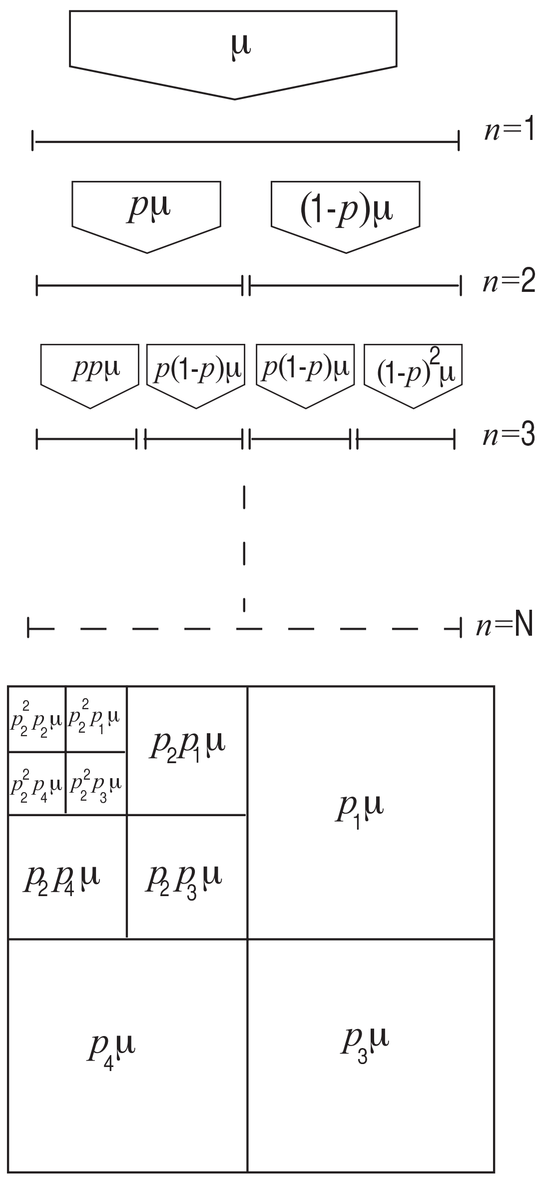

FIG. 1. Upper panel: Different steps of generating multifractal rough surface in one dimension. Lower panel: The same steps for multifractal rough surface in two dimensions [11].

be calculated explicitly. The scaling exponent $\tau(q)$ is defined via a partition function as

$$Z_q(l) = \lim_{l\to 0} \sum_{i=1}^{n(l)} |P(\mathcal{A}_i,l)|^q \sim l^{\tau(q)}. \qquad (4)$$

Using the value of $P(\mathcal{A})$, e.g., for the binomial cascade model $P(\mathcal{A}) = \frac{1}{2}[\delta(\mathcal{A}-p)+\delta(\mathcal{A}-(1-p)]$, one finds

$$\tau(q) = \lim_{l\to 0} \frac{\ln(Z_q(l))}{\ln(l)} = (E-1)(q-1) - \log_2[p^q + (1-p)^q], \qquad (5)$$

where E is the dimension of the geometric support, where for our rough surfaces is $E = 2$. For the generalized p model, the analytic expression of the multifractal scaling exponent in two dimensions is given by [45]

$$\tau(q) = -\log_2\left(p_1^q + p_2^q + p_3^q + p_4^q\right). \qquad (6)$$

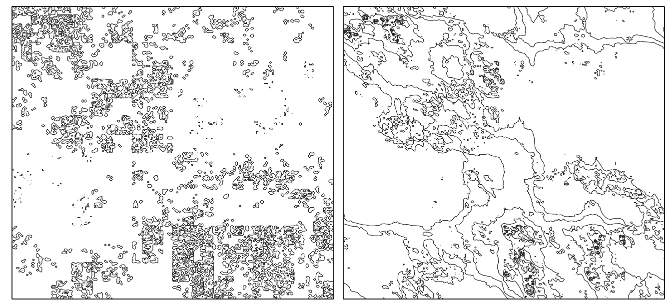

FIG. 2. Left: Contour plot at some typical levels of a singular multifractal rough surface generated by the binomial cascade multifractal method with $p = 0.22$ ($H = 0.803$). The right panel indicates the contour lines of the same surface convolved with $H^* = 0.700$. The system size is 256×256.

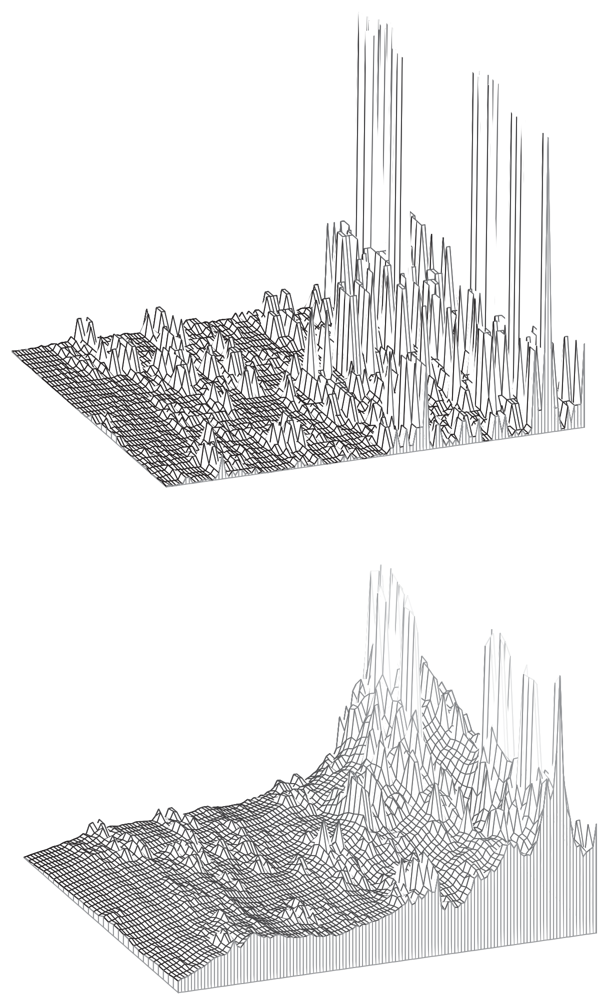

FIG. 3. Upper panel: A part of height fluctuations of singular measure mentioned in Fig. 2. Lower panel: The same surface convolved with $H^* = 0.700$.

One can use the above theoretical expression to get the most relevant quantities of the multifractal behavior and check the reliability and robustness of the numerical method.

Recently, factorial moments, G moments, correlation integrals, void probabilities, combinants, and wavelet correlations have been used to examine many interesting features of multiplicative cascade processes [46]. But there is some ambiguity in the properties of such processes that represent multifractal phenomena. On the other hand, sensitivity and accuracy of results are method dependent; consequently, it is highly advised to simultaneously use various tools in order to ensure the reliability of given results for underlying multifractal rough features. Moreover, to make a relation between experimental data and simulation, generally, we require more than one characterization [31,47].

In the next section, to investigate the multifractal properties of simulated rough surfaces in two dimensions, we will introduce the so-called multifractal detrended fluctuation analysis.

III. MULTIFRACTALITY OF SYNTHESIS ROUGH SURFACE

There are many different methods to determine the multiscaling properties of real as well as synthetic multifractal surfaces such as spectral analysis [48], fluctuation analysis [49], detrended fluctuation analysis (DFA) [6,50,51], wavelet transform module maxima (WTMM) [9,10,13,52,53], and discrete wavelets [54,55]. For real data sets and in the presence of noise, the multifractal DFA (MF-DFA) algorithm gives very reliable results [34,50]. Since it does not require the modulus maxima procedure, this method is simpler than WTMM; however, it involves a bit more effort in programming.

In this work, we rely on the two-dimensional multifractal detrended fluctuation analysis (MF-DFA) to determine the spectrum of the generalized Hurst exponent, $h(q)$. We then compare the given results with the theoretical prediction to check the reliability of our simulation. Suppose that for a rough surface in two dimensions the height of the fluctuations is represented by $\mathcal{H}(\mathbf{r})$ at coordinate $\mathbf{r} = (i,j)$ with resolution Δ. The MF-DFA in two dimensions has the following steps [34].

Step 1. Consider a two-dimensional array $\mathcal{H}(i,j)$, where $i = 1,2,\ldots,M$ and $j = 1,2,\ldots,N$. Divide the $\mathcal{H}(i,j)$ into $M_s \times N_s$ nonoverlapping square segments of equal sizes $s \times s$, where $M_s = [\frac{M}{s}]$ and $N_s = [\frac{N}{s}]$. Each square segment can be denoted by $\mathcal{H}_{\nu,w}$ such that $\mathcal{H}_{\nu,w}(i,j) = \mathcal{H}(l_1 + i, l_2 + j)$ for $1 \leqslant i,j \leqslant s$, where $l_1 = (\nu - 1)s$ and $l_2 = (w - 1)s$.

Step 2. For each nonoverlapping segment, the cumulative sum is calculated by

$$Y_{\nu,w}(i,j) = \sum_{k_1=1}^{i}\sum_{k_2=1}^{j} \mathcal{H}_{\nu,w}(k_1,k_2), \tag{7}$$

where $1 \leqslant i,j \leqslant s$.

Step 3. Calculating the local trend for each segments by a least-squares of the profile, linear, quadratic or higher-order polynomials can be used in the fitting procedure as follows:

$$\mathcal{B}_{\nu,w}(i,j) = ai + bj + c, \tag{8}$$

$$\mathcal{B}_{\nu,w}(i,j) = ai^2 + bj^2 + c. \tag{9}$$

Then determine the variance for each segment as follows:

$$\mathcal{D}_{\nu,w}(i,j) = Y_{\nu,w}(i,j) - \mathcal{B}_{\nu,w}(i,j), \tag{10}$$

$$F^2_{\nu,w}(s) = \frac{1}{s^2}\sum_{i=1}^{s}\sum_{j=1}^{s} \mathcal{D}^2_{\nu,w}(i,j). \tag{11}$$

A comparison of the results for different orders of the DFA allows one to estimate the type of the polynomial trends in the surface data.

Step 4. Averaging over all segments to obtain the qth-order fluctuation function,

$$F_q(s) = \left(\frac{1}{M_s \times N_s}\sum_{\nu=1}^{M_s}\sum_{w=1}^{N_s}\left[F^2_{\nu,w}(s)\right]^{q/2}\right)^{1/q}, \tag{12}$$

where $F_q(s)$ depends on scale s for different values of q. It is easy to see that $F_q(s)$ increases with increasing s. Notice that $F_q(s)$ depends on the order q. In principle, q can take any real value except zero. For $q = 0$, Eq. (12) becomes

$$F_0(s) = \exp\left[\frac{1}{2M_s \times N_s}\sum_{\nu=1}^{M_s}\sum_{w=1}^{N_s}\ln F^2_{\nu,w}(s)\right]. \tag{13}$$

For $q = 2$ the standard DFA in two dimensions will be retrieved.

Step 5. Finally, investigate the scaling behavior of the fluctuation functions by analyzing log-log plots of $F_q(s)$ versus s for each value of q,

$$F(s) \sim s^{h(q)}. \tag{14}$$

The Hurst exponent is given by

$$H \equiv h(q = 2) - 1. \tag{15}$$

Using standard multifractal formalism [50] we have

$$\tau(q) = qh(q) - E. \tag{16}$$

It has been shown that for very large scales, $N/4 < s$, $F_q(s)$ becomes statistically unreliable because the number of segments N_s for the averaging procedure in step 4 becomes very small [34]. Thus, scales $N/4 < s$ should be excluded from the fitting procedure of determining $h(q)$. On the other hand, one should be careful also about systematic deviations from the scaling behavior in Eq. (12) that can occur for the small scales $s < 10$.

The singularity spectrum, $f(\alpha)$, of a multifractal rough surface is given by the Legendre transformation of $\tau(q)$ as

$$f(\alpha) = q\alpha - \tau(q), \tag{17}$$

where $\alpha = \frac{\partial\tau(q)}{\partial q}$. It is well known that for a multifractal surface, various parts of the feature are characterized by different values of α, causing a set of Hölder exponents instead of a single α. The interval of Hölder spectrum, $\alpha \in [\alpha_{\min},\alpha_{\max}]$, can be determined by [56,57]

$$\alpha_{\min} = \lim_{q\to+\infty}\frac{\partial\tau(q)}{\partial q}, \tag{18}$$

$$\alpha_{\max} = \lim_{q\to-\infty}\frac{\partial\tau(q)}{\partial q}. \tag{19}$$

To evaluate the statistical errors due to numerical calculations we introduce posterior probability distribution function in terms of likelihood analysis. To this end, suppose the measurements and model parameters are assigned by $\{X\}$ and $\{\Theta\}$, respectively. The conditional probability of the model parameters for a given observation are as follows (posterior):

$$P(\Theta|X) = \frac{\mathcal{L}(X|\Theta)P(\Theta)}{\int \mathcal{L}(X|\Theta)P(\Theta)d\Theta}. \tag{20}$$

here $\mathcal{L}(X|\Theta)$ and $P(\Theta)$ are called Likelihood and prior distribution, respectively. The prior distribution containing all initial constraints regarding model parameters. Based on the central limit theorem, the likelihood function can be given by a product of Gaussian functions as follows:

$$\ln \mathcal{L}(X|\Theta) \sim \frac{-\chi^2(\Theta)}{2}, \tag{21}$$

where, e.g., for determining $h(q)$ we have $\{X\} : \{F_q(s)\}$ as the observations and $\{\Theta\} : \{h(q)\}$ as the free parameter to be determined. Also,

$$\chi^2(h(q)) = \sum_s \frac{[F_{\rm obs}(s) - F_{\rm the}(s;h(q))]^2}{\sigma^2_{\rm obs}(s)}, \tag{22}$$

where $F_{\rm obs}(s)$ is computed by Eqs. (12) and (13). $F_{\rm the}(s;h(q))$ is the fluctuation function given by Eq. (14). The observational error is $\sigma_{\rm obs}(s)$. By using the Fisher matrix, one can evaluate the value of the error bar at a 1σ confidence interval of $h(q)$ [58]

$$\mathcal{F}(q) \equiv \left\langle \frac{\partial^2 \ln \mathcal{L}}{\partial h(q)^2} \right\rangle \tag{23}$$

and

$$\sigma(q) \simeq \frac{1}{\sqrt{\mathcal{F}(q)}}. \tag{24}$$

Finally, we report the best value of the scaling exponent at a 1σ confidence interval according to $h(q) \pm \sigma(q)$. Using the method mentioned in the previous section, we simulated multifractal rough surfaces and checked their multifractality nature by using the spectrum of $h(q)$. Figure 4 shows the generalized Hurst exponent and $\tau(q)$ as a function of q for various values of measure sets reported in Table I. The subindex ($i \in [1,12]$) of each H_i (Hurst exponent) throughout this paper corresponds to a given set of p values reported in Table I. In addition, the singularity spectrum of a typical simulated multifractal rough surface has been shown in the lower panel of Fig. 4. The q dependence of $h(q)$ as well as the extended range of singularity spectrum demonstrate the multifractality nature of synthesis rough surfaces. The theoretical predictions of $\tau(q)$, $h(q)$, and $f(\alpha)$ shown by the solid lines in the corresponding plots are given by Eqs. (6), (16), and (17), respectively. There is a good consistency between the theoretical predictions and the computational values.

Before going further, it is worth mentioning that in the cascade p model for various sets of p values that have the same $h(q=2)$, in principle, there exist different $h(q)$ spectrua. To show this point, we fixed the value of $\tau(q=2)$ in Eq. (6) and by having, e.g., p_1 and p_2, one can compute the rest of the p values according to the normalization of the p's. In

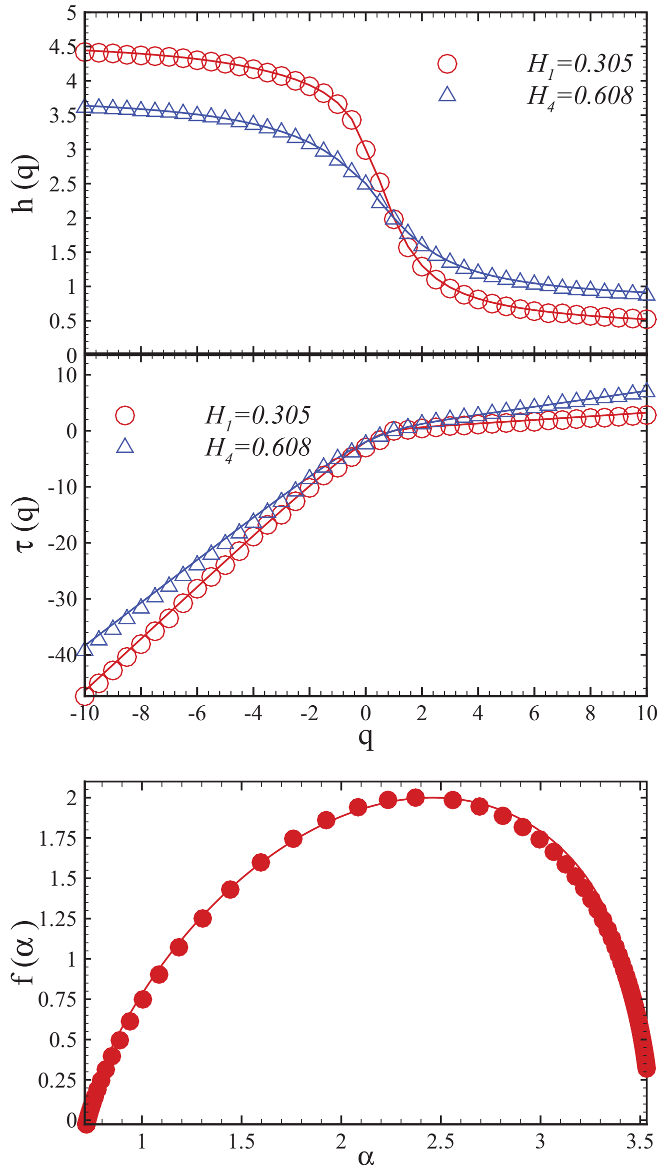

FIG. 4. (Color online) Diagrams of $h(q)$ (upper panel) and $\tau(q)$ (middle panel) for different surfaces. We have distinguished different surfaces with their $H_i = h_i(q=2) - 1$ from Table I. The subindex ($i \in [1,12]$) of each H_i (Hurst exponent) throughout this paper corresponds to a given set of p values reported in Table I. The lower panel corresponds to the singularity spectrum of a typical multifractal rough surface with $H_4 = 0.608$. In all diagrams, symbols and solid lines correspond to results given by numerical calculation and theoretical formulas, respectively.

Fig. 5 we show the MF-DFA results of various sets of p values causing the same so-called $h(q=2)$ exponents. Subsequently, it is expected that for characterizing the geometrical properties of underlying surfaces, one must take into account the full spectrum of generalized Hurst exponents.

It must be pointed out that the generated surfaces have some discontinuities (see Fig. 2). To make them smooth, a proper way is to use a fractionally integrated singular cascade (FISC) method [10]. In this method, the multifractal measure is transformed into a smoother multifractal rough surface by

TABLE I. The p values used for construction of surfaces with various Hurst exponents, $H_i = h_i(q=2) - 1$. The subindex ($i \in [1,12]$) of H_i represents the label of different sets of p values.

Hurst exponent	p_1	p_2	p_3	p_4
$H_1 = 0.305$	0.040	0.800	0.080	0.080
$H_2 = 0.404$	0.100	0.740	0.080	0.080
$H_3 = 0.504$	0.120	0.680	0.110	0.090
$H_4 = 0.608$	0.190	0.610	0.130	0.070
$H_5 = 0.608$	0.090	0.100	0.610	0.200
$H_6 = 0.608$	0.600	0.100	0.237	0.063
$H_7 = 0.608$	0.350	0.100	0.546	0.004
$H_8 = 0.706$	0.210	0.550	0.130	0.110
$H_9 = 0.802$	0.220	0.480	0.200	0.100
$H_{10} = 0.697$	0.120	0.180	0.560	0.140
$H_{11} = 0.806$	0.160	0.180	0.170	0.490
$H_{12} = 0.906$	0.410	0.200	0.210	0.180

filtering the singular multifractal measure [$\mu(\mathbf{r})$; Eq. (1)] in the Fourier space as

$$\mathcal{H}(\mathbf{r}) = \mu(\mathbf{r}) \otimes |\mathbf{r}|^{-(1-H^*)}, \tag{25}$$

where $\otimes$ is the convolution operator and $H^* \in (0,1)$ is the order of smoothness (see the right panel of Fig. 2 and the lower panel of Fig. 3). In this case, $\tau_f(q)$ reads as

$$\tau_f(q) = \tau(q) + qH^*, \tag{26}$$

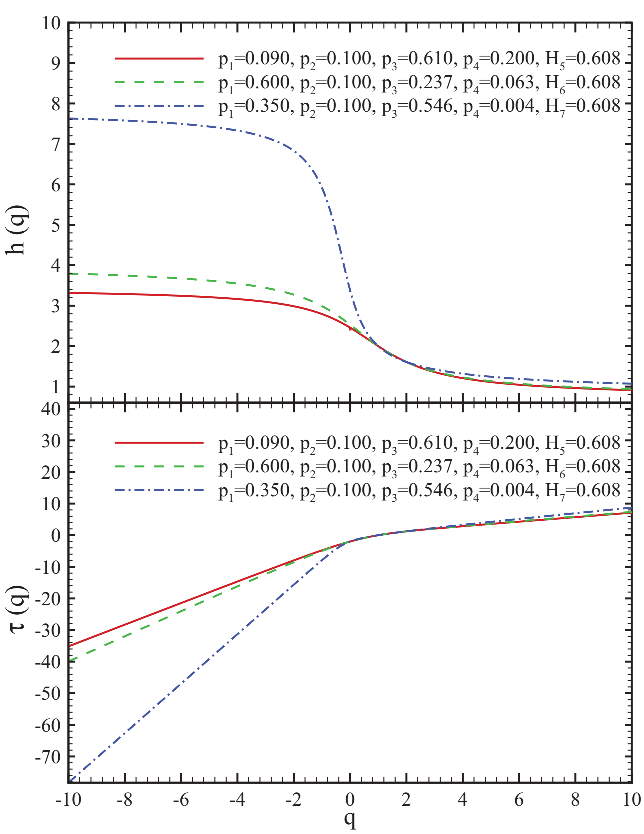

FIG. 5. (Color online) The multifractal spectrum of surfaces produced by different sets of p values but with the same $h(q=2)$ up to our numerical precision.

TABLE II. The most relevant exponents concerning stochastic processes in one and two dimensions.

Exponent	1D-fGn	1D-fBm	2D-Cascade	2D-fBm
γ	$2-2H$	$-2H$	$1-2H$	$-1-2H$
β	$2H-1$	$2H+1$	$2H$	$2H+2$

where $\tau(q)$ is given by Eq. (6). Using the correlation function, $C(|\mathbf{r}|) \sim |\mathbf{r}|^{-\gamma}$, and its Fourier transform one can derive the power spectrum scaling exponent β of the singular as well as the smoothened synthetic multifractal surfaces. To this end, we demand the scaling behavior for the power spectrum to be

$$S(k) \sim |\mathbf{k}|^{-\beta}, \tag{27}$$

where $\mathbf{k} = (k_x, k_y)$, $k_x = \frac{2\pi}{\Delta \times N} i$, $k_y = \frac{2\pi}{\Delta \times N} j$, and (i,j) run from 1 to $N = L/\Delta$ (the pixel of system size). Subsequently, the power spectrum scaling exponent is given by [10]

$$\beta = 1 + 2H^* - \log_2[p^2 + (1-p)^2]. \tag{28}$$

To make more sense, in Table II we collected the correlation and power spectrum exponents of stochastic processes in one and two dimensions.

Figure 6 indicates one-dimensional profiles obtained along a typical horizontal cut in Fig. 2 for singular and smoothened multifractal rough surfaces. The lower panels of Fig. 6 show the power spectrums of simulated rough surfaces. The convolution does not change the multifractality nature of singular measure (see Fig. 7). In this plot one can see that the synthetic smoothened surface remains multifractal.

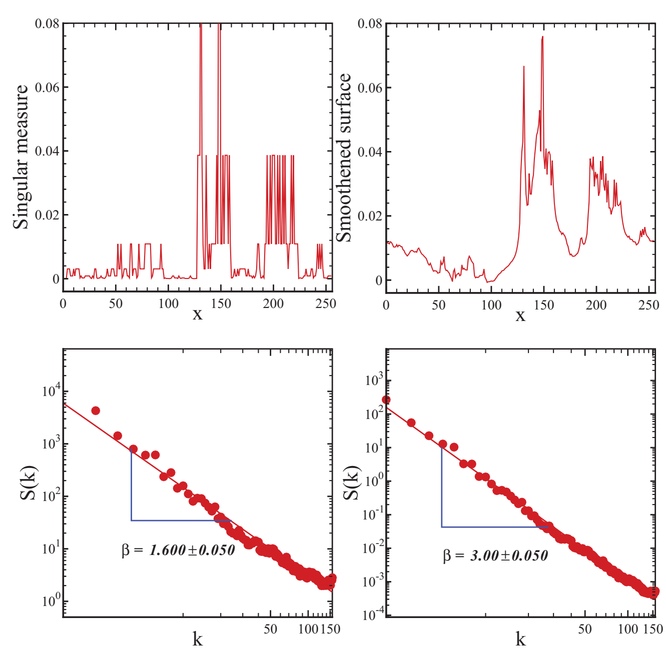

FIG. 6. (Color online) Upper panel: Profile of singular (left) and smoothened (right) multifractal rough surfaces along a typical horizontal cut in Fig. 2. Lower panel: Spectral density of mentioned mock rough surfaces. The solid lines in the lower panel corresponds to a power-law fitting function and symbols are given by numerical calculation. Here we took $H^* = 0.700$.

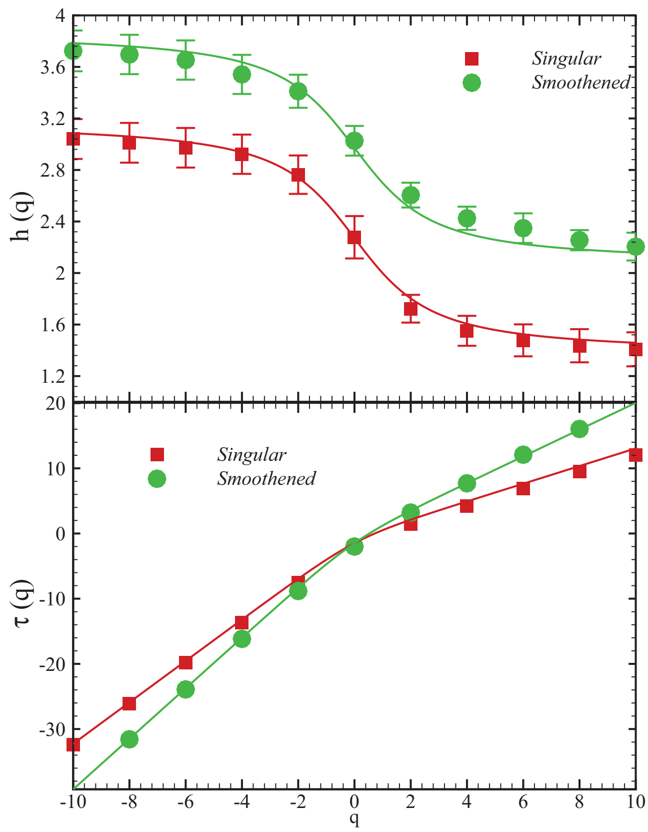

FIG. 7. (Color online) Generalized Hurst exponent of singular measure for $H_9 = 0.802$ (square symbols) and that of convolved with $H^* = 0.700$ (circle symbols). The solid lines are from the theory.

IV. GEOMETRICAL EXPONENTS OF CONTOUR LOOPS

For a given multifractal rough surface with the height $\mathcal{H}(\mathbf{x})$, a level set $\mathcal{H}(\mathbf{x}) = \mathcal{H}_0$ for different values of $\mathcal{H}_0$ consists of many closed nonintersecting loops. These loops are recognized as contour loops. The contour loop ensemble corresponds to contour loops of various level sets. In Fig. 2 we have plotted a set of contour loops at some typical levels for a singular multifractal rough surface and corresponding convolved surface with $H^* = 0.700$. The loop length s can be defined as the total number of unit cells constructing a contour loop multiplied by lattice constant Δ. The radius of a typical loop is represented by R and it is the side of the smallest box that completely enwraps the loop. For a monofractal surface, these loops are usually fractal and their size distribution is characterized by a few scaling functions and scaling exponents. For example, the contour line properties can be described by the loop correlation function $G(\mathbf{r})$. The loop correlation function measures the probability that the two points separated by the distance $\mathbf{r}$ in the plane lie on the same contour. Rotational invariance of the contour lines forces $G(\mathbf{r})$ to depend only on $r = |\mathbf{r}|$. This function for the contours on the lattice with grid size Δ and in the limit $r \gg \Delta$ has the scaling behavior

$$G(r) \sim r^{-2x_l}, \tag{29}$$

where x_l is the loop correlation exponent. It was shown numerically [27,30,31] that for all the known monofractal rough surfaces this exponent is superuniversal and equal to $\frac{1}{2}$. A key consequence of this result is that the contour loops with perimeter s and radius R of such surfaces are self-similar. When these lines are scale invariant, one can determine the fractal dimension as the exponent in the perimeter-radius relation. The relation between contour length s and its radius of gyration R is

$$\langle s\rangle(R) \sim R^{D_f}, \tag{30}$$

where D_f is the fractal dimension and R is defined by $R^2 = \frac{1}{N}\sum_{i=1}^{N}[(x_i - x_c)^2 + (y_i - y_c)^2]$, with $x_c = \frac{1}{N}\sum_{i=1}^{N} x_i$ and $y_c = \frac{1}{N}\sum_{i=1}^{N} y_i$ being the central mass coordinates. The D_f is the fractal dimension of one contour and for monofractal rough surfaces is given by $D_f = \frac{3-H}{2}$ [31]. Depending on what feature of the multifractal rough surface is under investigation one can get various types of fractal dimensions. In this paper we introduce the fractal dimension of an isoheight line, D_f, and the fractal dimension of all the level set, d. The generalized form of fractal dimension can be expressed by means of a partition function of the underlying feature, which is contours in this context, as

$$D(q) = \lim_{l\to 0} \frac{1}{q-1}\frac{\ln[Z_q(l)]}{\ln(l)}, \tag{31}$$

where l is the size of the cells that one uses to cover the domain and its minimum value is equal to grid size, Δ. $Z_q(l)$ is the partition function defined in Eq. (4) but here it should be constructed by using contour loops instead of a height function and q can be any real number. It is easy to show that $D(q = 0) = D_f$ and $D(q = 1)$ corresponds to the so-called entropy of underlying system [45].

For a given self-similar loop ensemble, one can define the probability distribution of contour lengths $\tilde{P}(s)$. This function is a measure for the total loops with length s and follows the power law

$$\tilde{P}(s) \sim s^{-\eta}, \tag{32}$$

where η is a scaling exponent. Another interesting quantity with the scaling property is the cumulative distribution of the number of contours with area greater than A which has the following form:

$$P_>(A) \sim A^{-\frac{\xi}{2}}. \tag{33}$$

For monofractal rough surfaces we have $\xi = 2 - H$. Using the scaling property of the monofractal surfaces it was shown that the three exponents D_f, η, ξ, and x_l satisfy the following hyperscaling relations [30]:

$$D_f = \frac{\xi}{(\eta - 1)}, \tag{34}$$

$$D_f = \frac{2x_l - 2}{\eta - 3}. \tag{35}$$

Using the above relations it is easy to get the relation between η and Hurst exponent H. Before closing this section, we summarize all of the exponents introduced in this section in Table III.

In the next section we will calculate all mentioned exponents by using different numerical methods for singular

TABLE III. The relevant exponents introduced in this paper to characterize synthetic multifractal rough surfaces.

Exponent	Relation	Description
x_l	$G(r) \sim r^{-2x_l}$	Loop correlation exponent
D_f	$\langle s\rangle(R) \sim R^{D_f}$	Fractal dimension of a contour loop
$D(q)$	Eq. (31)	Multifractal dimension
d	$N(l) \sim l^{-d}$	Fractal dimension of all contour set
η	$\tilde{P}(s) \sim s^{-\eta}$	Length distribution exponent
ξ	$P_>(A) \sim A^{-\frac{\xi}{2}}$	Area cumulative exponent

as well as smoothened multifractal rough surfaces and we will examine the validity of the hyperscaling relations in this context.

V. NUMERICAL RESULTS

In order to examine the geometrical exponents of the contour loops mentioned in Table III of synthetic multifractal rough surfaces, we have generated multifractal rough surfaces with different $h(q=2)$'s using the typical measures reported in Table I. We have generated 100 ensembles of each surface with various sizes ranging from (2048×2048) to (4096×4096). To extract the contour loops of the mock multifractal rough surfaces at mean height, $\mathcal{H}_0$, we use two different methods, the contouring algorithm and the Hoshen-Kopelman algorithm [26]. According to our results, these two methods give almost the same results for geometrical exponents. In the next subsections we present our numerical results concerning the exponents introduced in the preceding sections.

A. Loop correlation function exponent

The loop correlation function exponent x_l is the most central exponent in monofractal rough surfaces. It is independent of H and is equal to $\frac{1}{2}$. This result has also been proven for $H=0$ according to the exact solvable statistical mechanics model for contours equivalent to the critical $O(2)$ loop model on the honeycomb lattice [31,59].

To find the correlation function from a given loop ensemble for multifractal rough surfaces, we followed the algorithm described in Ref. [31]. We calculated the loop correlation function $G(r)$ for our multifractal rough surfaces (with system size 2048×2048 and averaging is done over 10 realizations). The log-log diagram of $G(r)r^{2x_l}$ versus r for different sets of p values ($H_i = h_i(q=2) - 1$ for some $i \in [1,12]$) are shown in Fig. 8. Each set corresponds to a synthetic multifractal rough surface generated according to the algorithm presented in Sec. II. Our results demonstrate that the x_l exponent depends not only on the value of the Hurst exponent but also on the different sets of p values (see the upper panel of Fig. 8). In other words, as reported in Table I as well as shown in upper panel of Fig. 8, the sets $i=4$, $i=5$, and $i=6$ of p values have equal Hurst exponents; nevertheless, the corresponding correlation exponents, x_l, for these sets differ completely. On the other hand, at the level of our numerical accuracy, as shown in the lower panel of Fig. 8, the value for the smoothened multifractal surfaces correlation exponents is the same as that reported for the monofractal rough surfaces, namely $x_l = \frac{1}{2}$.

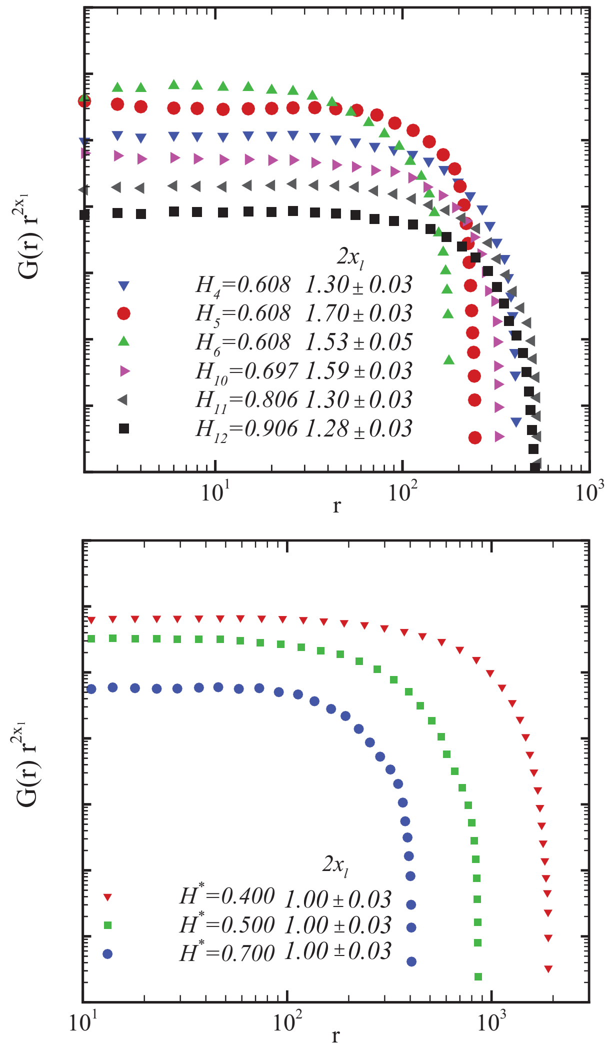

FIG. 8. (Color online) Log-log diagram of $r^{2x_l}G(r)$ versus r for different Hurst exponents. The upper panel corresponds to singular measure with the sets of p values reported in Table I. The lower panel indicates the loop correlation function for smoothened multifractal surface for various H^*'s. In these figures we shifted the y axis vertically. The system size is 4096×4096.

B. Fractal dimension

To calculate the fractal dimension of a contour loop, we have calculated the perimeter and radius of gyrations of different contour loops. Figure 9 shows log-log plot of $\langle s\rangle(R)$ versus $\langle R\rangle$ values for synthetic multifractal rough surfaces with typical value of Hurst exponent, $H_4 = 0.608$. There are two distinct regions with different slopes in the diagram; the first region is related to a large number of small loops with radius smaller than 1 ($R<1$) with $D_f = 1.00 \pm 0.01$. This is not a relevant phenomenon and it comes from the contouring algorithm that produces lots of contour loops around very small clusters (made usually from one cell). In the second region ($R>1$), the slope increases to 1.43 ± 0.02 and it maintains the scaling behavior up to very large sizes. The slopes for the different Hurst exponents follow the relation $D_f = (3-H)/2$ for the monofractal case [31]. For various values of the Hurst exponent our computation is shown in

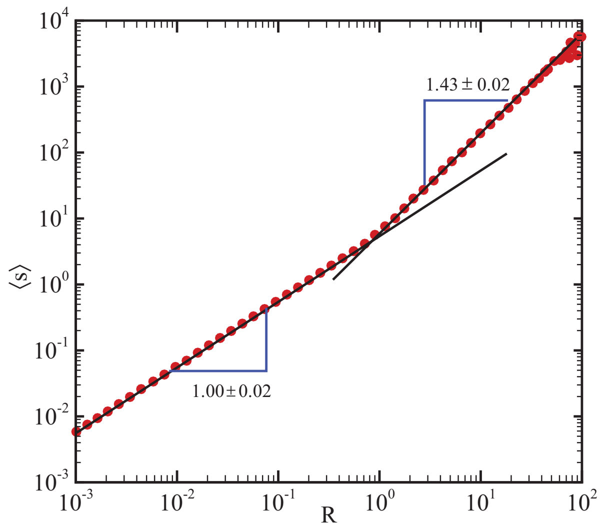

FIG. 9. (Color online) The log-log plot of $\langle s\rangle(R)$ versus R for a synthetic multifractal singular rough surface for $H_4 = 0.608$.

the upper panel of Fig. 10 (see also Table IV). At the 1σ confidence interval all slopes are the same. On the contrary, in the case of the contour lines of the convolved rough surfaces with arbitrary H^*'s the fractal dimension of a contour line follows the formula of a monofractal surface with $H = H^*$, namely $D_f = (3 - H^*)/2$. It is quite interesting that these results are completely independent form the p values (lower panel of Fig. 10). This simply means that the fractal dimension of the contour loops of the singular rough surfaces does not change with respect to the $h(q = 2)$. In other words, in contrast to the monofractal case, $h(q = 2)$ alone cannot represent the properties of the underlying singular multifractal rough surface.

We also calculated the fractal dimension by using partition function introduced in Eqs. (4) and (31). Figure 11 shows $D(q)$ as a function of q. The q dependence of these results confirms that contour loops of synthetic singular and smooth multifractal rough surfaces are multifractal. For $q = 0$ at a 68% confidence interval $D(q = 0) = 1.46 \pm 0.05$. This is also in agreement with the value determined by calculating the scaling behavior of the contour sizes. In addition, as we may expect, this diagram demonstrates that the isoheight contour loops of

TABLE IV. Different geometrical exponents of the contour loops extracted from surfaces with different sets of p values reported in Table I. Theses values are completely dependent on the p values.

H	η	D_f	ξ	$2x_l$
$H_1 = 0.305$	2.67 ± 0.03	1.43 ± 0.04	2.44 ± 0.06	1.60 ± 0.10
$H_2 = 0.404$	2.60 ± 0.03	1.41 ± 0.04	2.30 ± 0.06	1.49 ± 0.10
$H_3 = 0.504$	2.50 ± 0.03	1.42 ± 0.04	2.16 ± 0.06	1.25 ± 0.05
$H_4 = 0.608$	2.45 ± 0.02	1.42 ± 0.04	2.04 ± 0.06	1.30 ± 0.03
$H_5 = 0.608$	2.74 ± 0.02	1.43 ± 0.04	2.50 ± 0.06	1.70 ± 0.03
$H_6 = 0.608$	2.64 ± 0.02	1.42 ± 0.04	2.31 ± 0.06	1.53 ± 0.03
$H_8 = 0.706$	2.35 ± 0.02	1.43 ± 0.04	1.90 ± 0.06	1.12 ± 0.03
$H_9 = 0.802$	2.27 ± 0.02	1.44 ± 0.04	1.80 ± 0.06	1.02 ± 0.03

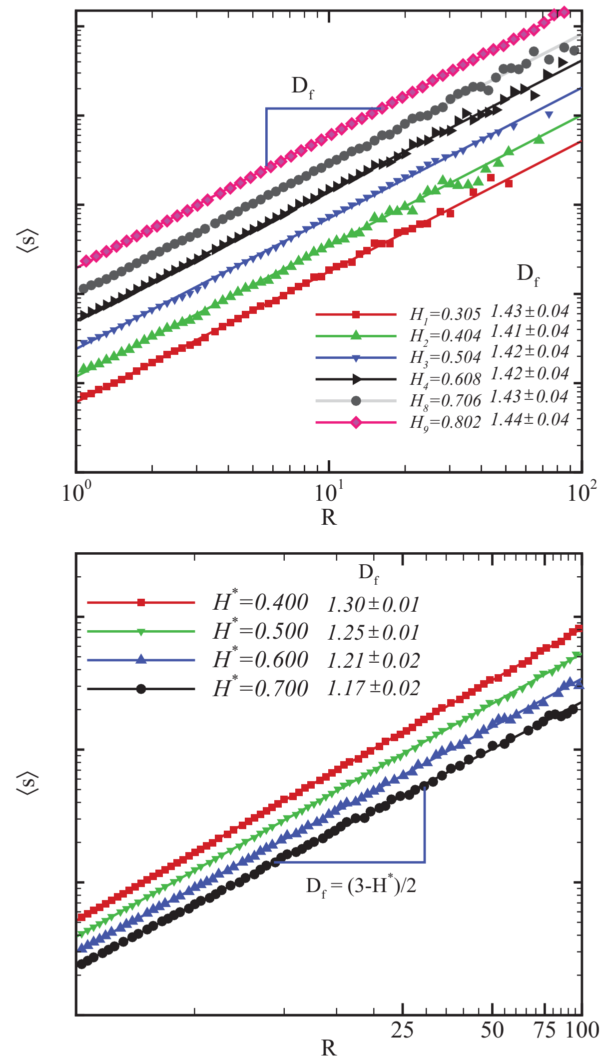

FIG. 10. (Color online) Upper panel: log-log of $\langle s\rangle(R)$ versus R for singular multifractal rough surfaces for various sets of p values reported in Table I. Lower panel: The same diagram for smoothened synthetic multifractal rough surfaces. The sample size is 4096×4096 and the ensemble average was done over 100 realizations. To make more sense, we shifted the values of $\langle s\rangle$ vertically for different multifractal rough surfaces.

underlying simulated multifractal rough surfaces behave as a multifractal feature.

As mentioned, the fractal dimension of all the contours, d, differs from the fractal dimension of a contour loop, D_f. The fractal dimension of a contour set for monofractal rough surfaces is given by $d = 2 - H$. For the smoothened multifractal rough surfaces introduced by Eq. (25), the fractal dimension of the contour set is $d = 2 - H^*$ [13]. We have calculated the fractal dimension of the contour set by using the box counting method. As previously, we used a least-squares equation [Eq. (21)] to determine the slope in the log-log diagram of the number of segments that will cover the underlying feature $N(l)$ versus length scale l for different Hurst exponents. To obtain the best-fit value for the slope corresponding to our data, as well as its error, we divided the data into different ranges and determined the slope by

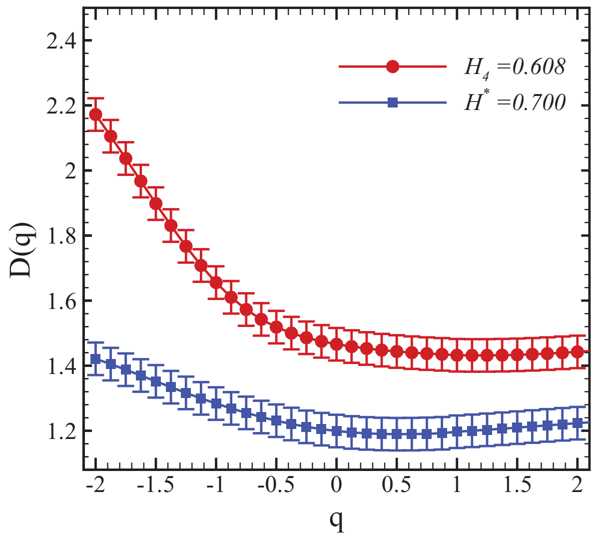

FIG. 11. (Color online) Generalized fractal dimension versus q for singular measure with $H_4 = 0.608$ and for smoothened multifractal surface which has been generated by convolution of singular measure with $H^* = 0.700$. For singular and smoothened surfaces $D_f = 1.46 \pm 0.05$ and $D_f = 1.19 \pm 0.05$, respectively.

least-squares method. To do so according to the likelihood function [Eq. (21)], we define χ^2 as

$$\chi^2(d) = \sum_{i=1}^{\mathcal{N}} \frac{[N(l_i) - N_{\mathrm{theor}}(l_i;d)]^2}{\sigma(l_i)^2}, \tag{36}$$

where $\mathcal{N}$ is the number of partitioning, namely $\mathcal{N} = L/l_{\mathcal{N}}$, $N_{\mathrm{theor}}(l_i;d) \sim l_i^{-d}$, and $\sigma^2(l_i)$ is the variance of the data in the corresponding range. Finally, we determined the minimum χ^2 and the best slope for the data. Figure 12 corresponds to synthetic smoothened multifractal rough surfaces. In addition, we checked that whether the result associated to the smoothened rough surfaces depends on the set of p values correspond to the

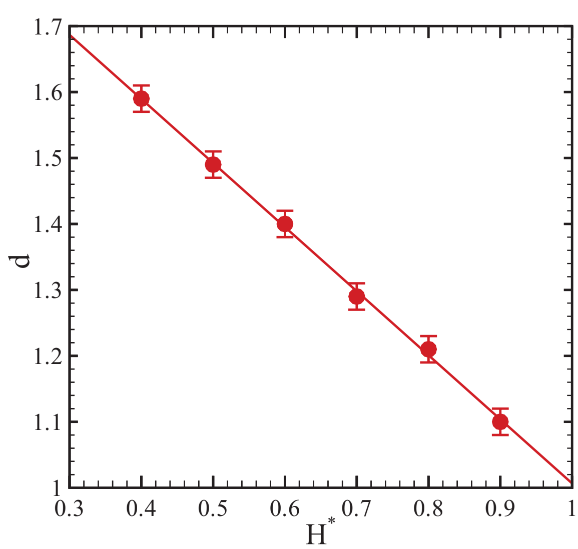

FIG. 12. (Color online) Fractal dimension of all contours of the smoothened multifractal surfaces as a function of H^*. The solid line corresponds to the linear fitting function.

same value of $h(q=2)$. Our findings confirm that d does not depend on different sets of p values. However, for the singular measure, d depends on the value of H and even p's used for the cascade algorithm. It has no regular behavior with respect to $h(q=2)$. Moreover, for various sets of p values giving the same value of $h(q=2)$, one finds different values for fractal dimensions of all contour sets. This is quite surprising because for the singular measure multifractal surface, we have $H^* = 0$ and, therefore, if the formula $2 - H^*$ was correct in this regime, we should have $d = 2$ for all the different $h(q=2)$'s. We are not aware of any theoretical argument that can explain this phenomenon.

C. Cumulative distribution of areas

To calculate the exponent ξ we have calculated the $P_>(A)A^{\xi/2}$ with respect to the area of the contour loops. In Fig. 13 and Table IV we have shown the results for

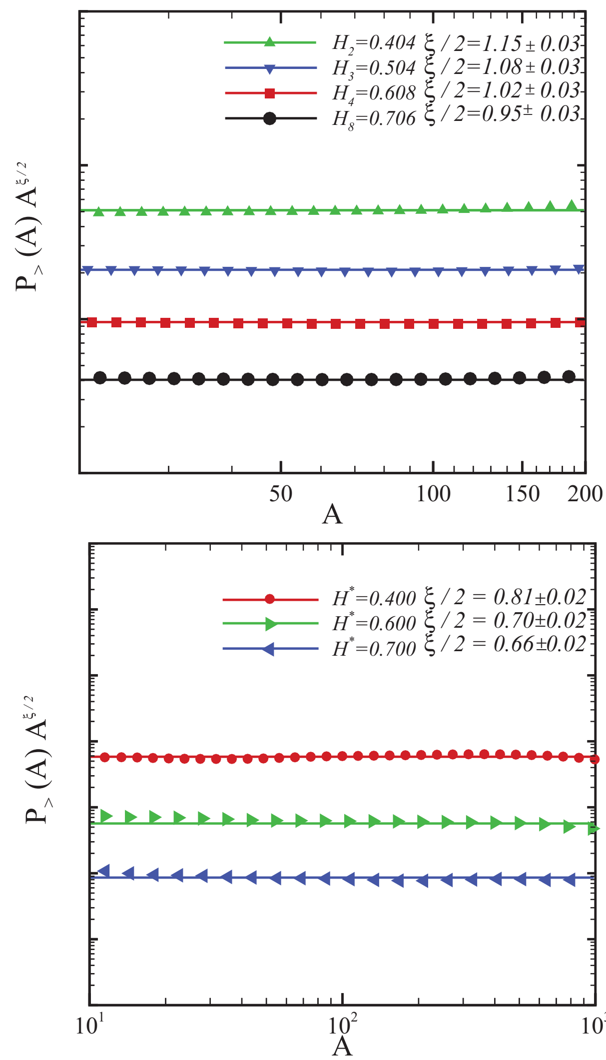

FIG. 13. (Color online) Upper panel: The cumulative distributions of the areas of the contour loops with respect to the area for the singular multifractal rough surfaces. The corresponding set of p values is given in Table I. Lower panel: The same distribution for the smoothened multifractal surfaces. For clarity, we shifted the value of the y axis vertically for both diagrams.

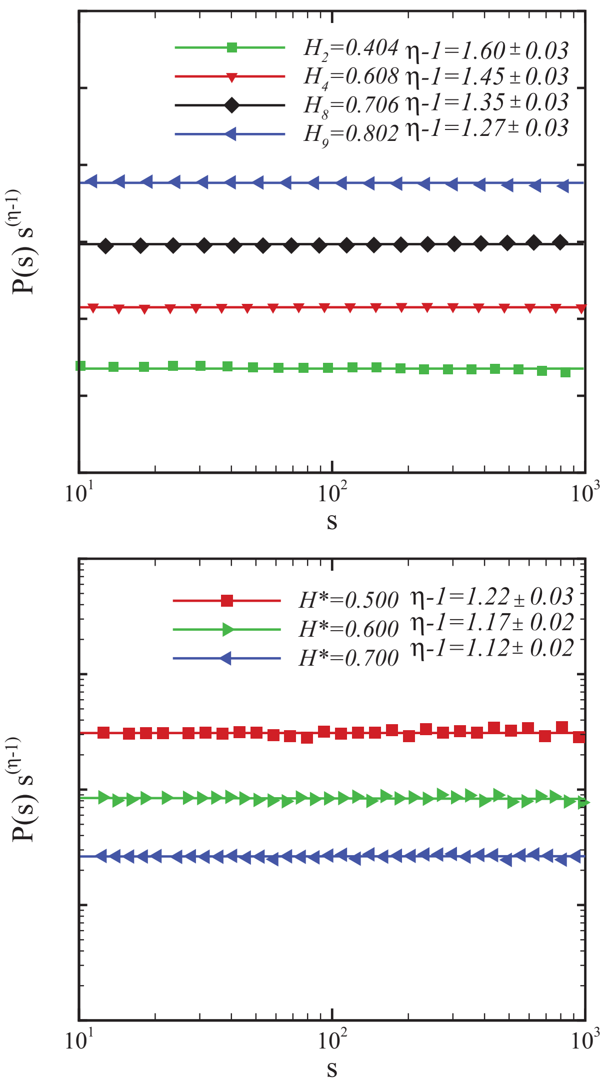

FIG. 14. (Color online) Upper panel: The perimeter distribution exponent for different sets of p values of the singular measure. Lower panel: The same measure for the smoothened multifractal rough surfaces. The values of the y axis are shifted vertically.

various values of the Hurst exponent reported in Table I and averaging is done over 100 realizations. The results differ markedly from what we expect for monofractal rough surfaces. For monofractal rough surfaces we have $\xi = 2 - H$. It must be pointed out that for synthetic singular multifractal rough surfaces ξ decreases by increasing H, which is the same as monofractal rough surfaces. In addition, ξ not only depends on $h(q = 2)$ but also is affected by other values of $h(q)$. This finding is due to the multifractality nature of the singular measure rough surface. The same computation for the smoothened multifractal rough surfaces is shown in the lower panel of Fig. 13. These results confirm that the exponent is controlled by H^*, and ξ is given by the same equation as for the monofractal rough surfaces.

D. Probability distribution of contour length

Final remarks concern the probability distribution of contour length. To this end, we investigated the logarithmic

TABLE V. Verification of two basic hyperscaling relations for synthetic singular measure multifractal rough surfaces.

H	$\eta - 1$	$\frac{\xi}{D_f}$	$3D_f + 2x_l$	$D_f\eta + 2$
$H_1 = 0.305$	1.67 ± 0.03	1.71 ± 0.06	5.89 ± 0.16	5.82 ± 0.12
$H_2 = 0.404$	1.60 ± 0.03	1.63 ± 0.06	5.72 ± 0.16	5.67 ± 0.12
$H_3 = 0.504$	1.50 ± 0.03	1.52 ± 0.06	5.51 ± 0.13	5.55 ± 0.11
$H_4 = 0.608$	1.45 ± 0.02	1.44 ± 0.06	5.56 ± 0.12	5.48 ± 0.10
$H_5 = 0.608$	1.74 ± 0.02	1.75 ± 0.06	5.99 ± 0.12	5.92 ± 0.11
$H_6 = 0.608$	1.64 ± 0.02	1.63 ± 0.06	5.79 ± 0.12	5.75 ± 0.11
$H_8 = 0.706$	1.35 ± 0.02	1.33 ± 0.06	5.41 ± 0.12	5.36 ± 0.10
$H_9 = 0.802$	1.27 ± 0.02	1.25 ± 0.05	5.34 ± 0.12	5.27 ± 0.10

diagram of $P(s)s^{\eta-1}$ versus s. We have depicted the results for the synthetic singular as well as smoothened multifractal surfaces for various values of $h(q = 2)$. For the smoothened multifractal rough surfaces, again, the exponents follow the behavior of the monofractal surfaces (see Fig. 14).

In spite of the huge difference between the geometrical exponents of the contour loops of the monofractal rough surfaces and singular multifractal rough surfaces, the hyperscaling relations $\frac{\xi}{D_f} = \eta - 1$ and $D_f = \frac{2x_l - 2}{\eta - 3}$ are valid up to numerical accuracy (see Table IV and Table V). The important factors in obtaining this hyperscaling relation concern power-law relations for $\tilde{P}(s)$ and $P_>(A)$. The second hyperscaling relation comes from the following equality:

$$\int_0^R G(r)d^2r \sim \int_0^\infty \min(s, R^{D_f})P(s)ds. \qquad (37)$$

Both sides are proportional to the mean of the length of that portion of the contour passing through origin that lies within a radius R from the origin [30].

VI. CONCLUSION

In this paper we have studied the contour lines of particular multifractal rough surfaces, namely the so-called multiplicative hierarchical cascade p model. Utilizing a stochastic cascade method [4,34], singular measure (original) and smoothened (convolved) multifractal rough surfaces with different Hurst exponents were generated. The $h(q)$ spectrums of these two-dimensional surfaces were determined by use of the MF-DFA method [34]. Then, by us of two different algorithms we generated the contour loops of the systems. Many different geometrical exponents, such as the fractal dimension of a contour loop, D_f, the fractal dimension of the contour set, d, the cumulative distributions of perimeters and areas, and the correlation exponents, x_l, were calculated for the singular and smoothened multifractal surfaces by use of different methods.

We summarize the most important results given in this study as follows. Our results confirmed that the exponent of the loop correlation function, x_l, for multifractal singular measures depends on p values. On the contrary, for multifractal smoothened surfaces, this value behaves the same as that for monofractal rough surfaces (see Fig. 8).

The scaling exponent of the size of the contours as a function of the radius representing fractal dimension, D_f, is

TABLE VI. A summarization of results given in this paper based on contouring analysis for synthetic singular and smoothened multifractal rough surfaces.

Exponent	Singular measure	Smoothened multifractal
x_l	Depends on p values	$\frac{1}{2}$
D_f	Identical	$\frac{3-H^*}{2}$
$D(q)$	Depends on q	Depends on q
d	Depends on p values	$2-H^*$
$\eta-1$	Depends on p values	$\frac{4-2H^*}{3-H^*}$
ξ	Depends on p values	$2-H^*$
$\frac{\xi}{D_f}=\eta-1$	Yes	Yes
$D_f=\frac{2x_l-2}{\eta-3}$	Yes	Yes

similar for various singular multifractal rough surfaces. But the relation between D_f and H^* for convolved multifractal surfaces is similar to monofractal surfaces. Nevertheless the contour loops have a multifractal nature (see Figs. 10 and 11).

The exponent of cumulative distribution of areas, ξ, for singular measure has multifractal nature. But for a smoothened surface, this quantity is controlled by H^* according to $\xi = 2-H^*$ and is completely independent of the p values (see Fig. 13).

Consequently, in the case of singular measure surfaces, all of the exponents show significant deviations from the well-known formulas for the monofractal rough surfaces. They depend on the generalized Hurst exponents, $h(q)$, whereas for convolved multifractal surfaces, all geometrical exponents are controlled by H^* according to a monofractal system. We emphasize that, interestingly, the hyperscaling relations, namely $\frac{\xi}{D_f}=\eta-1$ and $D_f=\frac{2x_l-2}{\eta-3}$ at the 1σ confidence interval, are valid for both singular and smoothened multifractal rough surfaces (see Table IV and V). In this system, which is labeled by H^*, many relevant properties are controlled by a few relations that have been presented for monofractal cases. However, singular and smoothened multifractal surfaces have a multifractal nature but, using a geometrical analysis, they belong to a different class, which is a nontrivial result. Table VI contains the most important results given in this paper.

Finally, to make this study more complete, it would be useful to extend this approach for various simulated rough surfaces by use of different methods and examine their hyperscaling relations. In addition, there are some methods to distinguish various multiplicative cascade methods, such as n-point statistics [60].

ACKNOWLEDGMENTS

We are grateful to M. Ghaseminezhad for cross-checking some of the results and also for fruitful discussions. M.S.M. and S.M.V.A. are grateful to the associate office of the ICTP and their hospitality. The work of S.M.V.A. was supported in part by the Research Council of the University of Tehran.

[1] D. Sornette, *Critical Phenomena in Natural Sciences: Chaos, Fractals, Selforganization and Disorder: Concepts and Tools* (Springer-Verlag, Heidelberg, 2000).
[2] H. E. Stanley and P. Meakin, Nature **335**, 405 (1988).
[3] M. Ausloos and D. H. Berman, Proc. R. Soc. London A **400**, 331 (1985).
[4] J. Feder, *Fractals* (Plenum Press, New York/London, 1988).
[5] Plamen Ch. Ivanov, Luis A. Nunes Amaral, Ary L. Goldberger, Shlomo Havlin, Michael G. Rosenblum, Zbigniew R. Struzik and H. Eugene Stanley, Nature **399**, 461 (1999).
[6] C.-K. Peng, S. V. Buldyrev, S. Havlin, M. Simons, H. E. Stanley, and A. L. Goldberger, Phys. Rev. E **49**, 1685 (1994).
[7] Armin Bunde, Jurgen Kropp, Hans-Joachim Schellnhuber, *The Science of Disasters: Climate Disruptions, Heart Attacks, and Market Crashes*, Vol. 2, (Springer, Berlin, 2002); Armin Bunde, Shlomo Havlin, *Fractals in Science* (Springer-Verlag, Berlin, 1994); S. Hosseinabadi, A. A. Masoudi, and M. S. Movahed, Physica B, **405**, 2072 (2010); Ajay Chaudhari, Gulam Rabbani, and Shyi-Long Lee, J. Chin. Chem. Soc. **54**(5), 1201 (2007); Ajay Chaudhari, Ching-Cher Sanders Yan, and Shyi-Long Lee, Appl. Surf. Sci. **238**, 513 (2004); M. Vahabi, G. R. Jafari, N. Mansour, R. Karimzadeh, and J. Zamiranvari, Journal of Statistical Mechanics: Theory and Experiment (JSTAT), P03002 (2008); Xia Sun, Zhuxi Fu, Ziqin Wu, Physica A **311**, 327 (2002).
[8] Pradipta Kumar Mandal and Debnarayan Jana, Phys. Rev. E **77**, 061604 (2008).
[9] A. Arneodo, N. Decoster, P. Kestener, and S. G. Roux, Adv. Imaging Electron Phys. **126**, 1 (2003).
[10] S. G. Roux, A. Arneodo, and N. Decoster, Eur. Phys. J. B **15**, 765 (2000); N. Decoster, S. G. Roux, and A. Arneodo, *ibid.* **15**, 739 (2000); A. Arnedo, N. Decoster, and S. G. Roux, *ibid.* **15**, 567 (2000).
[11] C. Meneveau and K. R. Sreenivasan, Phys. Rev. Lett. **59**, 1424 (1987); J. Fluid Mech. **224**, 429, (1991); K. R. Sreenivasan and R. A. Antonia, Annu. Rev. Fluid Mech. **29**, 435 (1997).
[12] R. Benzi, G. Paladin, G. Parisi, and A. Vulpiani, J. Phys. A: Math. Gen. **17**, 3521 (1984).
[13] J. F. Muzy, E. Bacry, and A. Arneodo, Phys. Rev. Lett. **67**, 3515 (1991).
[14] T. Vicsek, Physica A **168**, 490 (1990).
[15] E. Ben-Jacob, O. Shochet, A. Tenenbaum, I. Cohen, A. Czirok, and T. Vicsek, Fractals **2**, 15 (1994).
[16] S. Lovejoy, Science **216**, 185 (1982); R. F. Cahalan, in *Advances in Remote Sensing and Retrieval Methods*, edited by A. Deepak, H. Fleming, and J. Theon (Deepak Publishing, Hampton, VA, 1989), p. 371.
[17] M. S. Movahed, F. Ghasemi, S. Rahvar, and M. R. Tabar, Phys. Rev. E **84**, 021103 (2011).
[18] A. I. Zad, G. Kavei, M. R. R. Tabar, and S. M. V. Allaei, J. Phys. Condens. Matter **15**, 1889 (2003).
[19] J. D. Farmer, E. Ott, and J. A. Yorke, Physica D **7**, 153 (1983); Peter Grassberger and Itamar Procaccia, Phys. Rev. Lett. **50**, 346 (1983); R. Badii and A. Politi, *ibid.* **52**, 1661 (1984).

[20] M. Chekini, M. R. Mohammadizadeh, and S. M. V. Allaei, Appl. Surf. Sci. **257**, 7179 (2011).

[21] M. S. Movahed and E. Hermanis, Phys. A **387**, 915 (2008).

[22] J. W. Kantelhardt, e-print arXiv:0804.0747.

[23] B. Dubuc, J. F. Quiniou, C. Roques-Carmes, C. Tricot, and S. W. Zucker, Phys. Rev. A **39**, 1500 (1989); T. Higuchi, Physica D **46**, 254 (1990); N. P. Greis and H. S. Greenside, Phys. Rev. A **44**, 2324 (1991); W. Li, Int. J. Bifurcation Chaos **1**, 583 (1991); B. Lea-Cox and J. S. Y. Wang, Fractals **1**, 87 (1993).

[24] A. A. Saberi, M. A. Rajabpour, and S. Rouhani, Phys. Rev. Lett. **100**, 044504 (2008).

[25] A. A. Saberi, M. D. Niry, S. M. Fazeli, M. R. Rahimi Tabar, and S. Rouhani, Phys. Rev. E **77**, 051607 (2008).

[26] M. A. Rajabpour and S. M. Vaez Allaei, Phys. Rev. E **80**, 011115 (2009).

[27] M. G. Nezhadhaghighi and M. A. Rajabpour, Phys. Rev. E **83**, 021122 (2011).

[28] A. A. Saberi, H. Dashti-Naserabadi, and S. Rouhani, Phys. Rev. E **82**, 020101 (2010).

[29] A. A. Saberi, Appl. Phys. Lett. **97**, 154102 (2010).

[30] J. Kondev and C. L. Henley, Phys. Rev. Lett. **74**, 4580 (1995).

[31] J. Kondev, C. L. Henley, and D. G. Salinas, Phys. Rev. E **61**, 104 (2000).

[32] C. Zeng, J. Kondev, D. McNamara, and A. A. Middleton, Phys. Rev. Lett. **80**, 109 (1998).

[33] Ajay Chaudhari, Ching-Cher Sanders Yan, and Shyi-Long Lee, J. Phys. A: Math and Gen. **36**, 3757 (2003).

[34] Gao-Feng Gu and Wei-Xing Zhou, Phys. Rev. E **74**, 061104 (2006).

[35] D. Schertzer and S. Lovejoy, *In Turbulent and Chaotic Phenomena in Fluids*, edited by T. Tatsumi (North-Holland, New York, 1984), pp. 505–508.

[36] D. Schertzer and S. Lovejoy, J. Geophys. Res. **92**, 9693 (1987).

[37] D. Schertzer, S. Lovejoy, F. Schmitt, Y. Ghigirinskaya, and D. Marsan, Fractals **5**, 427 (1997).

[38] D. Schertzer and S. Lovejoy, *Fractals: Physical Origin and Consequences*, edited by L. Pietronero (Plenum, New York, 1989), p. 49.

[39] J. Wilson, D. Schertzer, and S. Lovejoy, *Fractals and Nonlinear Variability in Geophysics*, edited by D. Schertzer and S. Lovejoy (Kluwer, Dordrecht, 1991), p. 185.

[40] U. Frisch, *Turbulence* (Cambridge University Press, Cambridge, 1995).

[41] U. Frisch, P. L. Salem, and M. Nelkin, J. Fluid Mech. **87**, 719 (1978).

[42] W. Ochs and J. Wosiek, Phys. Lett. B **289**, 159 (1992); **305**, 144 (1993).

[43] Ph. Brax, J. L. Meunier and R. Peschanski, Z. Phys. C **62**, 649 (1994).

[44] Leandros Perivolaropoulos, Phys. Rev. D **48**, 1530 (1993).

[45] Thomas C. Halsey, Mogens H. Jensen, Leo P. Kadanoff, Itamar Procaccia, and Boris I. Shraiman, Phys. Rev. A **33**, 1141 (1986).

[46] Martin Greiner, Peter Lipa, and Peter Carruthers, Phys. Rev. E **51**, 1948 (1995); A. Bialas and R. Peschanski, Nucl. Phys. B **273**, 703 (1986); **308**, 857 (1988); C. B. Chiu and R. C. Hwa, Phys. Rev. D **43**, 100 (1991); S. Hegyi, Phys. Lett. B **309**, 443 (1993); H. C. Eggers, P. Lipa, P. Carruthers, and B. Buschbeck, Phys. Rev. D **48**, 2040 (1993).

[47] J. M. Gómez-Rodríguez, A. M. Baró, and R. C. Salvarezza, J. Vac. Sci. Technol. B **9**, 495 (1991).

[48] H. E. Hurst, Trans. Am. Soc. Civ. Eng. **116**, 770 (1951).

[49] C. K. Peng, S. Buldyrev, A. Goldberger, S. Havlin, F. Sciortino, M. Simons, and H. E. Stanley, Nature **356**, 168 (1992).

[50] J. W. Kantelhardt, S. A. Zschiegner, E. Koscielny-Bunde, S. Havlin, A. Bunde, and H. E. Stanley, Physica A **316**, 87 (2002).

[51] Kun Hu, Plamen Ch. Ivanov, Zhi Chen, Pedro Carpena, and H. E. Stanley, Phys. Rev. E **64**, 011114 (2001).

[52] Zbigniew R. Struzik, Arno P. J. M. Siebes, Physica A **309**, 388 (2002).

[53] J. Arrault, A. Arneodo, A. Davis, and A. Marshak, Phys. Rev. Lett. **79**, 75 (1997).

[54] J. W. Kantelhardt, H. E. Roman, and M. Greiner, Physica A **220**, 219 (1995).

[55] H. E. Roman, J. W. Kantelhardt, and M. Greiner, Europhys. Lett. **35**, 641 (1996).

[56] J. F. Muzy, E. Bacry, and A. Arneodo, Int. J. Bifurcation Chaos **4**, 245 (1994).

[57] A. Arneodo, E. Bacry, and J. F. Muzy, Physica A **213**, 232 (1994).

[58] B. A. Bassett, Y. Fantaye, R. Hlozek, and J. Kotze, e-print arXiv:0906.0993.

[59] B. Nienhuis, *Phase Transitions and Critical Phenomena*, Vol. 11, edited by C. Domb and J. L. Lebowitz (Academic Press, London, 1987).

[60] Martin Greiner, Hans C. Eggers and Peter Lipa, Phys. Rev. Lett. **80**, 5333 (1998).